

Enhancement of cutoff frequency for planar anisotropic Y_2Co_{17} by reductive diffusion method

Qianyang Zhou(周钱阳), Kai Long(龙凯), Rongfang Zhang(张榕芳), and Baorui Xia(夏宝瑞)
Citation: Chin. Phys. B, 2026, 35 (**8**): 087502. DOI: 10.1088/1674-1056/ae3064
http://cpb.iphy.ac.cn; http://iopscience.iop.org/cpb

What follows is a list of articles you may be interested in

Magnetic proximity-induced magnetoresistance in $Pt/Tm_3Fe_5O_{12}$ heterostructures

Zhengguo Liang(梁正国), Kunjie Dai(戴坤杰), Qiming Lv(吕崎鸣), Ao Wang(王傲), Jinfeng Zhang(章金凤), and Lingfei Wang(王凌飞)
Chin. Phys. B, 2026, 35 (**7**): 077512. DOI: 10.1088/1674-1056/ae5788

Prediction of material parameters of spin textures from LTEM images by machine learning models CNN and ViT

Bohan Li(李博涵), Xinyuan Zhang(张歆媛), Guanhua Chen(陈冠桦), and Lin Chen(陈琳)
Chin. Phys. B, 2026, 35 (**7**): 077507. DOI: 10.1088/1674-1056/ae5db1

Design of magnetoelectric coupling in ferroelectric metal

Wang Zhang(张旺) and Xue-Zeng Lu(逯学曾)
Chin. Phys. B, 2026, 35 (**7**): 077506. DOI: 10.1088/1674-1056/ae6173

MHz cut-off frequency and permeability mechanism of iron-based soft magnetic composites

Xiao-Wei Jin(金校伟), Tong Li(李通), Hui-Gang Shi(史慧刚), and De-Sheng Xue(薛德胜)
Chin. Phys. B, 2024, 33 (**9**): 097501. DOI: 10.1088/1674-1056/ad57aa

Zero-field skyrmions in FeGe thin films stabilized through attaching a perpendicularly magnetized single-domain Ni layer

Zi-Bo Zhang(张子博) and Yong Hu(胡勇)
Chin. Phys. B, 2021, 30 (**7**): 077503. DOI: 10.1088/1674-1056/abf4bc

---

Enhancement of cutoff frequency for planar anisotropic Y_2Co_{17} by reductive diffusion method

Qianyang Zhou(周钱阳)[1], Kai Long(龙凯)[1], Rongfang Zhang(张榕芳)[2,3], and Baorui Xia(夏宝瑞)[1,†]

[1] *Key Laboratory of Magnetism and Magnetic Functional Materials (Lanzhou University), Ministry of Education, School of Physical Science and Technology, Lanzhou University, Lanzhou* 730000, *China*

[2] *Key Laboratory of Western China's Environmental Systems (Ministry of Education) and Engineering Research Center of Fine Particle Pollution Control Technology and Equipment, Gansu Province, College of Earth and Environmental Sciences, Lanzhou University, Lanzhou* 730000, *China*

[3] *Gansu Agriculture Technology College, Lanzhou* 730000, *China*

(Received 2 July 2025; revised manuscript received 7 December 2025; accepted manuscript online 23 December 2025)

With the continuous development of wide-band-gap semiconductors such as silicon carbide and gallium nitride, power conversion electronic devices are required to operate at higher frequencies. Traditional magnetic materials are limited by Snoek's limit and cannot simultaneously achieve high permeability and high cutoff frequency; however, magnetic materials with planar anisotropy can overcome Snoek's limit. This work is devoted to the preparation of high-performance soft magnetic composite materials with high permeability, high cutoff frequency, and low losses to meet the requirements of high resonant frequency and device miniaturization. The rare-earth soft magnetic material Y_2Co_{17} was selected and prepared by the reduction diffusion method. The effects of ball milling time and ball-to-material ratio on the crystal structure and magnetic properties of Y_2Co_{17} were investigated to determine the optimum milling conditions that enable Y_2Co_{17} magnetic powder to exhibit excellent shape anisotropy and significantly increase the cutoff frequency. The results show that the shape anisotropy of Y_2Co_{17} magnetic powder is optimal when the ball milling time is 4 h and the ball-to-material ratio is 10:1, resulting in an increase in the cutoff frequency of the Y_2Co_{17}/epoxy composite to 170 MHz. This study demonstrates the promising potential of Y_2Co_{17}/epoxy composites for applications requiring high resonant frequency and device miniaturization.

Keywords: Y_2Co_{17}, cut-off frequency, Snoek's limit, plane anisotropy

PACS: 75.50.Bb, 75.40.Gb, 81.05.Bx, 75.30.Gw

DOI: 10.1088/1674-1056/ae3064 **CSTR:** 32038.14.CPB.ae3064

1. Introduction

Soft magnetic materials are a type of material that can rapidly respond to changes in external magnetic fields and achieve high magnetic induction intensity with low loss.[1] Due to their high sensitivity and low energy consumption, soft magnetic materials are widely used and currently include the largest variety of magnetic materials, including metallic soft magnetic materials, ferrite soft magnetic materials, and amorphous/nanocrystalline soft magnetic materials.[2–4] Metallic soft magnetic materials are often used in applications requiring high-efficiency magnetic properties, such as transformers, inductors, magnetic sensors, antennas, and wireless charging devices. However, the more severe skin effect and eddy current loss caused by their low resistivity limit their applications in the high-frequency band. Therefore, soft magnetic ferrite materials with higher resistivity are promising due to their superior high-frequency characteristics.[1] Although higher operating frequencies enable compact designs, high specific losses force designers to select lower operating flux densities, usually only 0.3–0.5 T, which increases the required volume and is not conducive to device miniaturization.[5,6] This limitation restricts their applications in fields requiring high magnetic flux density and high power.[5] Amorphous and nanocrystalline alloys are mostly formed as thin strips, which limits their compatibility in terms of shape and volume.[7] However, when fabricated into bulk forms, the relatively high eddy current loss also limits their applications, not to mention the relatively low saturation magnetization of nanocrystalline and amorphous soft magnetic materials. With the development of wide-band-gap semiconductor technology, it is becoming increasingly difficult for soft magnetic materials to meet the requirements for high resonant frequency and device miniaturization.[8–11]

In view of this, we aim to prepare soft magnetic composites with high permeability, high cutoff frequency, and low loss. Among these parameters, the cutoff frequency determines the frequency range over which magnetic materials can operate normally.[1] Generally, the working frequency of ferromagnetic materials cannot exceed the resonance frequency, because the largest energy loss occurs at resonance, as observed in magnetic spectrum curves. Thus, the natural resonance frequency is also called the cutoff frequency. For materials with uniaxial anisotropy, there is a competitive relationship between permeability and natural resonance frequency, which can be described by Snoek's limit.[12] For a material

†Corresponding author. E-mail: xiabr@lzu.edu.cn

© 2026 Chinese Physical Society and IOP Publishing Ltd. All rights, including for text and data mining, AI training, and similar technologies, are reserved.

with uniaxial anisotropy, Snoek's limit can be expressed as

$$(\mu_i - 1) f_r = 4\gamma M_s/3, \tag{1}$$

where μ_i is the initial permeability, f_r is the natural resonance frequency, γ is the gyromagnetic ratio, and M_s is the saturation magnetization. In other words, due to Snoek's limit, for a given magnetic material, it is impossible to increase the initial permeability and the natural resonance frequency simultaneously. However, for soft magnetic composites with easy-plane structures, the Snoek's limit can be overcome,[13] which can be described by

$$(\mu_i - 1) f_r = \left(\frac{\gamma M_s}{2}\right) \sqrt{H_\theta / H_\varphi}. \tag{2}$$

Here, H_θ and H_φ are the out-of-plane and in-plane anisotropy fields of the material, respectively. From Eq. (2), it can be seen that if the out-of-plane anisotropy of the material is much greater than its in-plane anisotropy, larger μ_i and f_r can be obtained simultaneously. Generally, planar anisotropy can be realized in two ways. One is that some materials with intrinsic magnetic crystal anisotropy can produce an easily magnetized surface, whose out-of-plane anisotropy is greater than the in-plane anisotropy. The other is that, due to shape anisotropy, the out-of-plane demagnetizing field of sheet magnetic materials is usually larger than the in-plane field, resulting in an easily magnetized surface.

Based on this, Y_2Co_{17} alloys are selected for investigation owing to their intrinsic magnetocrystalline anisotropy, which makes them planar-anisotropic materials. Furthermore, once the Y_2Co_{17} alloys are ground into sheets, their out-of-plane anisotropy field becomes the synergistic consequence of the magnetocrystalline anisotropy field and the shape anisotropy field. Thus, the right side of Eq. (2) would increase, and, promisingly, higher operating frequency and initial permeability can be obtained simultaneously.

To date, the main methods for synthesizing rare-earth alloys are metallothermic reduction and molten-salt electrolysis.[14] Light rare-earth metals such as La, Ce, Pr, and Nd are usually produced by molten salt electrolysis for economic and energy-efficiency reasons. The metallothermic reduction method is more suitable for synthesizing heavy rare-earth metals with higher melting and boiling points (Gd, Tb, and Y, etc.).[15] In this paper, the heavy rare-earth alloy Y_2Co_{17} was prepared by the reduction-diffusion method. The reduction-diffusion method reduces metal oxides to metals at one temperature and then allows them to react with Fe, Co, Ni, and other elements at another temperature to form the desired alloy.[16,17] It possesses several advantages as follows. First, it uses cheaper rare-earth oxides as raw materials instead of rare-earth metals, thus greatly reducing cost. Besides, it reduces pollution during smelting and homogenization and makes it easier to control the phase purity of the product.

In addition, metallic soft magnets inevitably exhibit eddy-current effects. Therefore, the cutoff frequency of Y_2Co_{17} is affected by eddy currents. To increase the cutoff frequency, it is necessary to fabricate uniform, micron-sized soft magnetic composite (SMC) particles.[18,19] The advantage of the reduction-diffusion method is that the particle size can be controlled by adjusting the size of the raw material particles, thus enabling the preparation of smaller particles to reduce the skin effect and improve the cutoff frequency.[18,19] In this work, the reduction-diffusion technique was employed to prepare Y_2Co_{17} particles with several-micron sizes and improved uniformity, thereby enhancing the cutoff frequency of the SMCs.

2. Experiment

During the experiment, the raw materials were commercially available Y_2O_3 powder (purity $> 99.9\%$), metallic Co, and Ca particles.

The chemical reaction equation for the preparation of Y_2Co_{17} alloy by the reduction-diffusion method is shown in

$$Y_2O_3 + 17Co + 3Ca = Y_2Co_{17} + 3CaO. \tag{3}$$

Y_2O_3 powder (purity $> 99.9\%$), metallic Co particles, and Ca particles were calculated and weighed according to the stoichiometric ratio of Eq. (3) for mixing. To compensate for potential volatilization losses during the reaction and ensure smooth progress, Y_2O_3 was weighed with a 5% excess, and excess Ca was added to ensure complete reduction. After completing the above steps, the powder was mixed in a three-dimensional mixer for 4 hours and pressed into a column weighing approximately 25 g. To prevent oxidation of the raw materials, the mixing process was performed under an argon atmosphere. The column was placed in an iron can and transferred to a vacuum tube furnace for reduction and diffusion. The iron can was sealed with CaO to prevent molten Ca leakage and avoid affecting the operation of the tube furnace. A mechanical pump was used to evacuate the system. During the tube furnace program, the temperature was first raised to 120 °C and maintained for a certain period, after which argon gas was introduced. Reduction-diffusion sintering was performed in an argon atmosphere by heating the sample to 880 °C and holding at this temperature for 4 hours. Subsequently, the temperature was increased to the diffusion temperature of 1080 °C and maintained for 8 hours for diffusion treatment. The sample was cooled in the furnace under an argon atmosphere to room temperature to obtain Y_2Co_{17} containing CaO. The prepared sample was roughly ground in a vacuum glove box, passed through a 200-mesh sieve, and then repeatedly washed with deionized water and ammonium acetate solution to obtain pure Y_2Co_{17} rare-earth soft magnetic powder. The drugs and equipment used in this experiment are listed in Tables 1 and 2.

Table 1. List of drugs used in the experiment.

Name	Purity	Manufacturer
Y_2O_3	99.5%	Tianjin Fengyue Chemical Co. LTD
Co	99.5%	Tianjin Guangfu Fine Chemical Co. LTD
Ca	99.5%	Shanghai McLean Biochemical Technology Co. LTD
CH_3COONH_3	98.0%	Sichuan Xilong Chemical Co. LTD
CH_3COCH_3	98.0%	Shanghai McLean Biochemical Technology Co. LTD
CH_3COOH	99.7%	Lianlong Bohua (Tianjin) Pharmaceutical and Chemical Co. LTD
Ar	99.99%	Lanzhou Yongfang Chemical Technology Co. LTD

Table 2. Equipment used in the experiment.

Name	Version	Manufacturer
3D motion mixer	GH-1-2L	Wenling Southern Powder Equipment Manufacturing Factory
Vacuum glove box	GBV-3	Changsha Tianchuang Powder Technology Co. LTD
Manual powder tablet press	769YP-24B	Tianjin Science And Technology High-tech Co. LTD
Muffle furnace	VBF-1200X	Hefei Kejing Material Technology Co. LTD
Vacuum tube furnace	BIF-1400C	Anhui BEC Equipment Technology Co. LTD
vacuum drying oven	DZF-6020	Hefei Kejing Material Technology Co. LTD

Flaky particles with a high aspect ratio (large lateral size relative to thickness) and pronounced morphological anisotropy can improve the magnetic permeability and cutoff frequency of Y_2Co_{17} magnetic powder. To obtain Y_2Co_{17} magnetic powder with a sheet-like particle morphology and improved magnetic properties, the powder was further ball-milled using a planetary ball mill. Ethanol was used as the grinding medium, and zirconia beads were used as the milling media. The ball mill speed was set to 400 r/min. The ball-milling time and ball-to-material ratio were selected as the experimental variables. Because the sintered powder contained CaO, ammonium acetate solution was used to remove CaO and obtain single-phase Y_2Co_{17}. Subsequently, the cleaned powder was dried in a vacuum drying oven and passed through a 200-mesh sieve to obtain Y_2Co_{17} rare-earth alloy powder. X-ray diffraction (XRD) and scanning electron microscopy (SEM) were used to characterize the crystal structure and microstructure of Y_2Co_{17}. The hysteresis loop of Y_2Co_{17} magnetic powder was measured using a vibrating sample magnetometer (the accuracy of the measured saturation magnetization was 1×10^{-6} emu) to determine the saturation magnetization and coercivity. To measure the magnetic properties, the Y_2Co_{17} powder was formed into a toroidal (ring-shaped) sample. Because Y_2Co_{17} powder lacks binding properties, epoxy resin was used as a binder. The milled powder was dried in a vacuum drying oven at 60 °C for 24 h and then mixed evenly with epoxy resin at a specified ratio using ultrasonication. After drying in a fume hood for 12 h, the composite was pressed using a tablet press at 10 MPa for 5 min and then at 20 MPa for 15 min to form dense discs. Subsequently, a Y_2Co_{17}/epoxy soft magnetic composite ring with an inner diameter of 7 mm and an outer diameter of 13 mm was fabricated using a mold. Finally, the permeability of the Y_2Co_{17}/epoxy soft magnetic composite ring was measured using an impedance analyzer. By analyzing the x-ray diffraction pattern, hysteresis loop, SEM image, and magnetic permeability spectrum of Y_2Co_{17} magnetic powder, the optimum milling conditions for achieving excellent shape anisotropy and high cutoff frequency were determined.

3. Result and discussion

3.1. Influence of milling time

The crystal structure of Y_2Co_{17} powders ball-milled for 2 h, 4 h, and 6 h was characterized by the XRD method, and the corresponding results are shown in Fig. 1. Y_2Co_{17} powder with 0 h milling represents the sample without ball milling. The results demonstrate that the diffraction peak positions of the Y_2Co_{17} magnetic powder after ball milling are essentially consistent with those of the standard JCPDS card for Y_2Co_{17} (No. 18-0434); however, the diffraction peak intensities are slightly reduced, and no obvious impurity peaks are observed. Meanwhile, the peak width of the main diffraction peak changes slightly when the milling time is increased from 4 h to 6 h. The above phenomenon is consistent with the potential XRD changes induced by internal stress. Microstrain and crystal defects are introduced as a result of internal stress. The diffraction peak width increases because the interplanar spacing is widened, while the diffraction intensity decreases because the crystal integrity is destroyed.

Figure 2 shows the static hysteresis loops of Y_2Co_{17} magnetic powder after ball milling for different times. The saturation magnetizations of Y_2Co_{17} powder milled for 2 h, 4 h, and 6 h are 0.9661×10^6 A/m, 0.9650×10^6 A/m, and 0.9647×10^6 A/m, respectively (Table 3). Compared with the test accuracy of the experimental equipment, the obtained data show only slight changes, which confirms the reliability of the

data. However, this slight decrease is more likely attributable to the incorporation of partially non-magnetic zirconia powder into Y_2Co_{17} during the ball milling process. Furthermore, the increase in coercivity of Y_2Co_{17} magnetic powder after ball milling may be related to internal stresses and defects introduced during the ball milling process.[20] The defects pin domain walls during the magnetization process, increasing the resistance to domain-wall motion and thus leading to decreased magnetic permeability and increased coercivity.[20] This explains the sharp increase in coercivity to over 200 Oe.

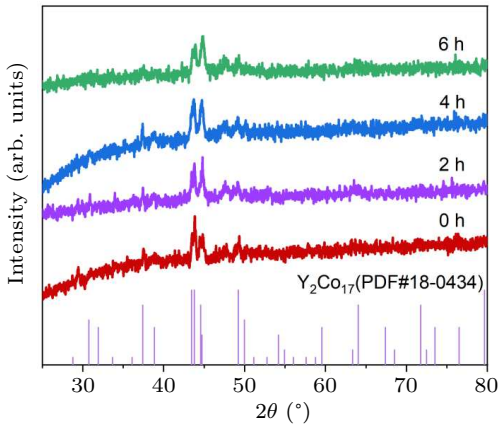


Fig. 1. X-ray diffraction patterns of Y_2Co_{17} materials at different ball-milling time.

SEM was used to characterize the microscopic morphology of Y_2Co_{17} magnetic powder before and after ball milling for different times, and the results are shown in Fig. 3. The formation and evolution of flaky structures can partially reflect changes in the shape anisotropy of Y_2Co_{17}. When the sample is not ball-milled, the particle morphology is basically spherical and more regular than that of the ball-milled samples, and no flaky structures appear. At a milling time of 2 h, the Y_2Co_{17} powder shows agglomeration with irregular particle shapes. As the milling time increases, some particles form flaky structures, while agglomerated clusters remain, resulting in the coexistence of particles and flakes at different milling times. However, clumps still remain, leading to the coexistence of particles and aggregates. When the milling time is increased to 6 h, the Y_2Co_{17} powder becomes predominantly granular, and the agglomerates are largely dispersed. This is because the flaky structures are further broken into granules, and the resulting particle size is smaller than that after 2 h of ball milling.

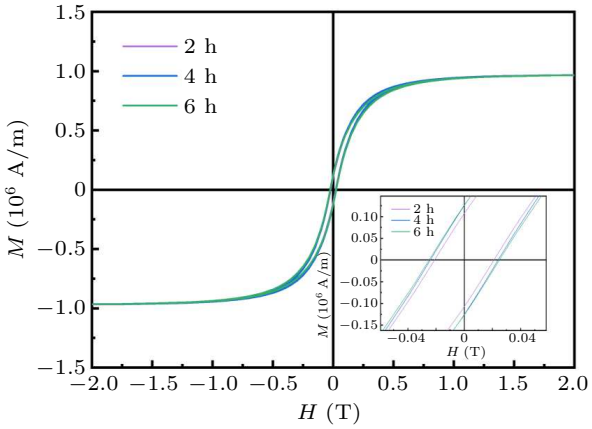


Fig. 2. Hysteresis loops of Y_2Co_{17} at different ball-milling time.

Table 3. The coercivity and saturation magnetization of Y_2Co_{17} magnetic powder with different ball milling time.

Ball milling time	H_c (Oe)	M (10^6 A/m)
2 h	210.17	0.9661
4 h	240.23	0.9650
6 h	249.09	0.9647

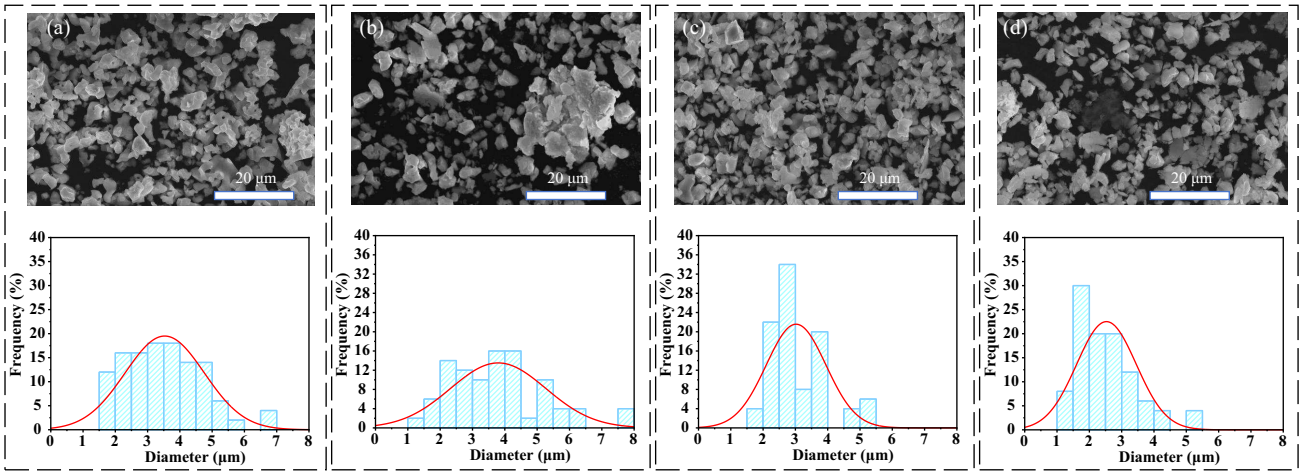


Fig. 3. SEM images of Y_2Co_{17} with different ball-milling times and the particle diameter distributions: (a) without ball milling, (b) ball milling for 2 h, (c) ball milling for 4 h, and (d) ball milling for 6 h.

Y_2Co_{17}/epoxy composites with a volume fraction of 33% were prepared by mixing Y_2Co_{17} magnetic powder samples and epoxy resin, respectively. Figure 4 shows the magnetic spectrum variation of Y_2Co_{17}/epoxy composites over the 1 MHz–1 GHz band. As the alternating magnetic field frequency increases, the real part of the permeability gradually

decreases, while the imaginary part initially increases and then decreases. This behavior reflects the dispersion and absorption characteristics of permeability.[1] When the imaginary part of the permeability reaches its maximum, the magnetic loss also reaches its maximum, and the corresponding frequency is the cutoff frequency of the magnetic material.[21] The cutoff frequencies of Y_2Co_{17} powder milled for 2 h, 4 h, and 6 h are 57.95 MHz, 171.75 MHz, and 31.62 MHz, respectively. Based on the above results, it can be concluded that the cutoff frequency first increases and then decreases with increasing milling time. Among them, the Y_2Co_{17}/epoxy sample milled for 4 h formed partially flaky particles with good shape anisotropy, and its cutoff frequency was the highest among all samples, reaching nearly 200 MHz. It should be noted that these frequencies were obtained at a ball-to-material ratio of 10:1 for all samples. It is also worth noting that the real part of the permeability falls below 1 at certain frequencies, likely due to the high magnetic anisotropy of rare-earth cobalt intermetallic compounds. Furthermore, core loss is a critical parameter for practical applications and can be deduced from the permeability spectrum according to[22]

$$\mu'' = \frac{P}{\pi f \mu_0 H_m^2}. \tag{4}$$

Therefore, comparison of the imaginary part of the permeability in the magnetic spectrum reveals that Y_2Co_{17} milled for 4 h exhibits the lowest power loss below the cutoff frequency.

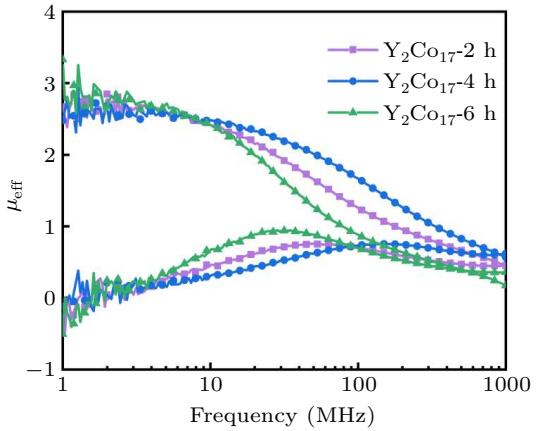


Fig. 4. Magnetic permeability spectra of Y_2Co_{17}/epoxy composites at different ball-milling times in the frequency range of 1 MHz–1 GHz.

3.2. The influence of the ball-to-material ratios

As one of the most important working parameters of ball milling, the ball-to-material ratio directly affects the grinding efficiency. Only with an appropriate ball-to-material ratio can the grinding media be effectively involved in the grinding process, fully enabling the impact and shear interactions between the grinding media and the material.[23–25] To determine the appropriate ball-to-material ratio, the Y_2Co_{17} magnetic powder was ball-milled at ball-to-material ratios of 5:1, 10:1, 25:1, and 40:1, respectively.

The XRD results of the material after ball milling show the XRD patterns of Y_2Co_{17} magnetic powder ball-milled with different ball-to-material ratios (Fig. 5). The results show that the diffraction peak positions of Y_2Co_{17} magnetic powder after ball milling are essentially consistent with those of the standard JCPDS card (No. 18-0434), indicating that the crystal structure of Y_2Co_{17} remains unchanged after ball milling and that the material retains good crystallinity. The primary diffraction peaks of the sample with a ball-to-material ratio of 25:1 exhibit reduced intensity and increased broadening. This is likely due to the increased structural homogeneity of the material during the ball milling process.

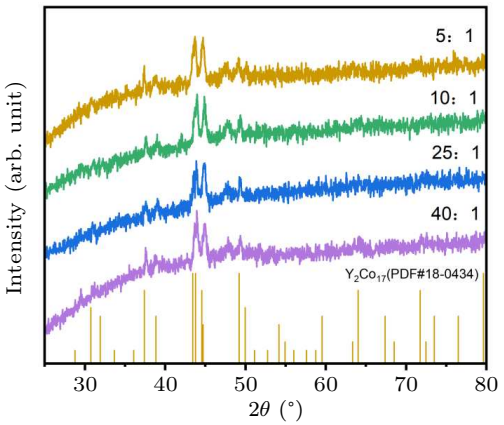


Fig. 5. XRD patterns of Y_2Co_{17} powders prepared with different ball-to-material ratios.

Figure 6 shows the static hysteresis loop of Y_2Co_{17} magnetic powder at different ball-to-material ratios. The results show that too large or too small a ball-to-material ratio will affect the milling efficiency and thereby affect the saturation magnetization. Only an appropriate ball-to-material ratio can ensure that Y_2Co_{17} powder maintains good soft magnetic properties, that is, high saturation magnetization and low coercivity. Specifically, with the gradual increase of the ball-to-material ratio, the saturation magnetization of Y_2Co_{17} magnetic powder initially increases, as shown in Fig. 6. After ball milling, at a ball-to-material ratio of 25:1, the saturation magnetization of Y_2Co_{17} magnetic powder reaches the maximum value of 0.9937×10^6 A/m. However, when the ball-to-material ratio is 40:1, the saturation magnetization of Y_2Co_{17} particles decreases to 0.9345×10^6 A/m. Meanwhile, the coercivity of Y_2Co_{17} magnetic powder decreases with increasing ball-to-material ratio. The results are shown in Table 4.

Table 4. The coercivity and saturation magnetization of Y_2Co_{17} magnetic powder with different ball-to-material ratio.

The ball-to-material ratio	H_c (Oe)	M (10^6 A/m)
5:1	224.84	0.9250
10:1	200.33	0.9632
25:1	211.85	0.9937
40:1	204.73	0.9345

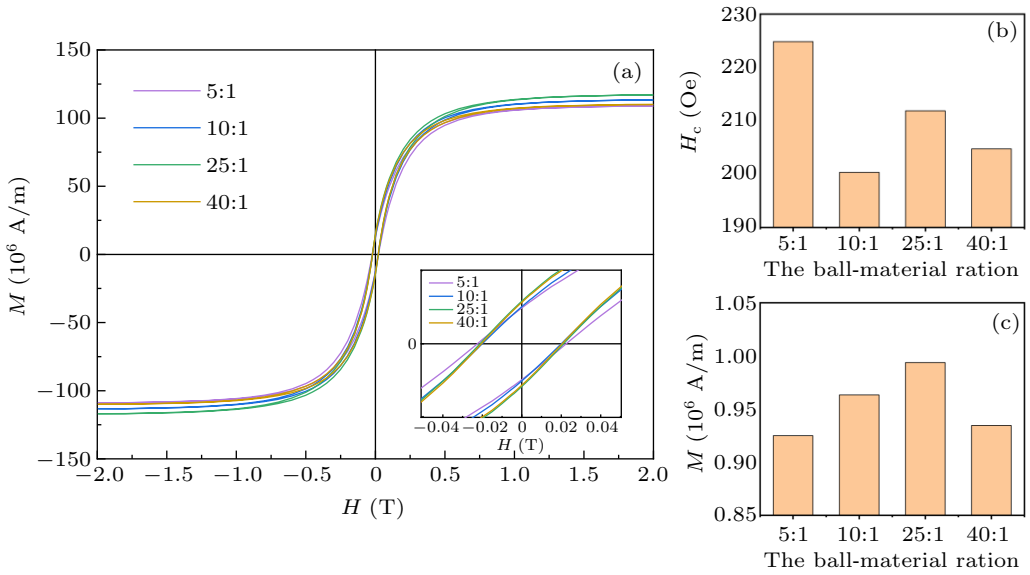


Fig. 6. (a) Hysteresis loops of Y_2Co_{17} material prepared with different ball-to-material ratios; (b) bar charts of H_c; (c) bar charts of M.

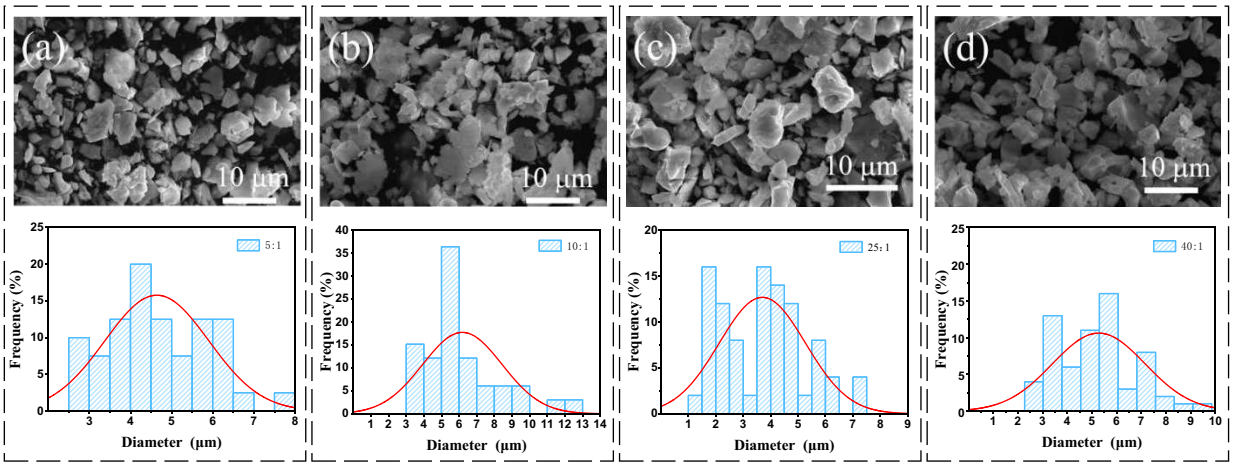


Fig. 7. SEM images of Y_2Co_{17} materials with different ball-to-material ratios and particle diameter distributions: (a) ball-to-material ratio of 5:1, (b) ball-to-material ratio of 10:1, (c) ball-to-material ratio of 25:1, and (d) ball-to-material ratio of 40:1.

As the ball-to-material ratio increases, the saturation magnetization first increases and then decreases. In fact, a higher ball-to-material ratio indicates more frequent collisions between balls and between balls and the material. When the ratio increases from 5:1 to 25:1, the mechanical alloying effect during ball milling leads to an increase in saturation magnetization.[26,27] However, when the ratio further increases to 40:1, the increased collision frequency may cause abrasion of the zirconia grinding balls, contaminating the Y_2Co_{17} sample and resulting in a decrease in saturation magnetization. Therefore, the saturation magnetization of Y_2Co_{17} powder at a ball-to-material ratio of 5:1 is low, and its soft magnetic properties are also poor. The ball-milled Y_2Co_{17} sample at a ball-to-material ratio of 25:1 exhibits high saturation magnetization, but its coercivity is also high, which adversely affects its soft magnetic properties. The sample at a ball-to-material ratio of 40:1 is also limited by low saturation magnetization and poor soft magnetic properties. Only at the appropriate ball-to-material ratio of 10:1 does Y_2Co_{17} magnetic powder exhibit optimally low coercivity and high saturation magnetization, resulting in the best soft magnetic properties.

Figure 7 shows SEM micrographs of Y_2Co_{17} magnetic powder after ball milling for 4 h at different ball-to-material ratios. At the ball-to-material ratio of 5:1, the Y_2Co_{17} powder contains predominantly large particles and few flaky particles, with an average particle size below 5 μm. When the ball-to-material ratio increased to 10:1, the Y_2Co_{17} magnetic powder exhibited a pronounced flaky structure, with particle sizes mainly distributed between 5–7 μm, and the thickness-to-diameter ratio was relatively small. Because Y_2Co_{17} is relatively brittle, increasing the ball-to-material ratio to 25:1 and 40:1 results in particles that are again irregular in shape, which may be attributed to the higher ball-to-material ratio. In fact, a higher ball-to-material ratio indicates more frequent collisions between the balls and the powder. As the ratio in-

creases, the flaky particles are further fragmented into irregular particles by high-frequency impacts; this change in particle morphology may affect eddy-current behavior. Under high-frequency conditions, eddy-current losses suppress magnetic moment rotation, leading to a significant reduction in resonance frequency. Therefore, the cutoff frequency of the Y_2Co_{17} sample with a ball-to-material ratio of 25:1 is expected to be reduced. The magnetic-spectrum results shown in Fig. 8 support this interpretation.

To investigate the effect of changes in the ball-to-material ratio on the high-frequency performance of Y_2Co_{17}, we measured the complex permeability spectrum of a Y_2Co_{17}/epoxy composite as a function of frequency using an impedance analyzer from 1 MHz to 1 GHz. The impedance-analyzer results in Fig. 8 show that, with the Y_2Co_{17} volume fraction held at 33% and samples ball-milled for 4 h at different ball-to-material ratios, the real part of the complex permeability (μ') of the Y_2Co_{17}/epoxy composite is about 2.6, and both μ' and the imaginary part (μ'') gradually decrease with increasing frequency.

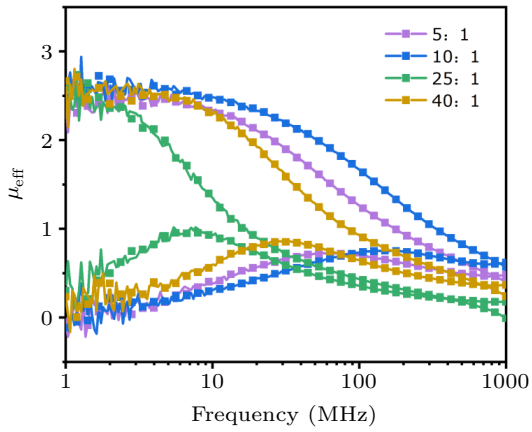


Fig. 8. Magnetic permeability spectra of Y_2Co_{17}/epoxy resin composites in the frequency range of 1 MHz to 1 GHz with different ball-to-material ratios.

Based on the imaginary part of the complex permeability, the cutoff frequencies of the samples with ball-to-material ratios of 40:1 and 5:1 are 28.51 MHz and 56.88 MHz, respectively. For the 25:1 ball-to-material ratio, the cutoff frequency of the Y_2Co_{17}/epoxy composite is low, only 7.16 MHz, likely due to magnetostatic interactions and particle shape. As shown in Fig. 7, at a ball-to-material ratio of 10:1, the Y_2Co_{17}/epoxy composite exhibits pronounced flaky particles with strong shape anisotropy, which increases the equivalent field of out-of-plane anisotropy and thus raises the cutoff frequency to nearly 170 MHz. Furthermore, the Y_2Co_{17} sample with a ball-to-material ratio of 10:1 also features the lowest power loss, as evidenced by its minimal imaginary part of the permeability prior to the cutoff frequency.

In fact, the cutoff frequency of the sample with a ball-to-material ratio of 10:1 is very close to that of the sample ball-milled for 4 h. This is because the ball-to-material ratio that yields the highest cutoff frequency is the same as the ratio used in the experiments investigating the effect of milling time on the cutoff frequency.

4. Conclusion

In summary, based on the idea that combining the magnetocrystalline anisotropy of Y_2Co_{17} powder with the shape anisotropy of flaky particles can increase the cutoff frequency of Y_2Co_{17}, we synthesized Y_2Co_{17} powder by the reduction-diffusion method and determined the conditions for increasing its cutoff frequency. We studied the effects of milling time and ball-to-material ratio on the crystal structure and magnetic properties of Y_2Co_{17} powder. Under identical processing conditions, both the milling time and ball-to-material ratio play essential roles in determining the powder's soft magnetic properties. The experimental results show that, at a ball milling time of 4 h and a ball-to-material ratio of 10:1, the material exhibits pronounced shape anisotropy, and the cutoff frequency of the Y_2Co_{17}/epoxy composite increases to approximately 170 MHz.

Acknowledgments

Project supported by the Natural Science Foundation of Gansu Province, China (Grant Nos. 23JRRA1368 and 23JRRA1109), the National Natural Science Foundation of China (Grant No. 12004146), the Key R & D projects in Gansu Province (Grant No. 23YFGA0002), and the Talent Scientific Fund of Lanzhou University.

References

[1] Che S L 2024 *Materials* **17** 89
[2] Liu Y P and He S J 2008 *J. Magn. Magn. Mater.* **320** 3318
[3] Stoppels D 1996 *J. Magn. Magn. Mater.* **160** 323
[4] Krings A, Boglietti A, Cavagnino A and Sprague S 2017 *IEEE Trans. Ind. Electron.* **64** 2405
[5] Xia N H, Chen M Q, Mao X K, Yan S and Ma H Q 2024 *J. Power Electron.* **24** 1374
[6] Kauder T and Hameyer K 2017 *IEEE Trans. Magn.* **53** 1
[7] Grundy P J 1980 *J. Magn. Magn. Mater.* **21** 1
[8] Zhao J, Wu C, Luo D H and Yan M 2019 *J. Magn. Magn. Mater.* **481** 140
[9] Silveyra J M, Ferrara E, Huber D L and Monson T C 2018 *Science* **362** 418
[10] Kroposki B, Pink C, DeBlasio R, Thomas H, Simoes M and Sen P K 2010 *IEEE Trans. Energy Convers.* **25** 901
[11] Houbi A, Aldashevich Z A, Atassi Y, Telmanovna Z B, Saule M and Kubanych K 2021 *J. Magn. Magn. Mater.* **529** 167839
[12] Zhao Y T, Liu L, Han J V, Wu W H and Tong G X 2017 *J. Alloys Compd.* **728** 100
[13] Tan G G, Zhang Y B, Qiao L, Wang T, Wang J B and Li F S 2015 *Phys. B* **477** 52
[14] Liao C F, Que L H, Fu Z H, Deng P, Li A L, Wang X and Chen S M 2024 *Metals* **14** 407
[15] Liu H, Zhang Y, Luan Y K, Yu H M and Li D Z 2020 *Metals* **10** 1376
[16] Chen H B, Zheng J W, Qiao L, Ying Y, Jiang L Q and Che S L 2018 *Rare Met.* **37** 989
[17] Liu D H, Lan Q F, Xie Z Y, Meng Y N, Zhang X L, Niu F and Yang Y M 2021 *Mater. Sci. Eng., B* **274** 115447

[18] Feng H, Jin X W, Li T, Cui H X, Meng C, Liu Z C and Xue D S 2025 *J. Alloys Compd.* **1014** 178742

[19] Qiao L, Tu C F, Wu W, Wang W B, Yang S Y, Sun Z, Wu P, Yang J B, Wang C S, Wang T and Li F S 2023 *Chin. Phys. B* **32** 054202

[20] Ma Y G, Qiao L, Zheng Z Y, Hao H B, Wang H, Sun Z, Tu C F, Wang T, Yang Z and Li F S 2023 *Chin. Phys. B* **32** 084202

[21] Wang Y K, Zhang P Y, Liu Z, Li K W, Xian C, Yang W Y, Luo Z C, Liu S Q, Han J Z, Du H L, Wang C S and Yang J B 2023 *AIP Adv.* **13** 025240

[22] Miyazaki T H 2012 *The Physics of Ferromagnetism* (Berlin: Springer Science & Business Media) pp. 11–85

[23] Hussain M, Oku Y, Nakahira A and Niihara K 1996 *Mater. Lett.* **26** 177

[24] Li Z J, Chen L, Chang F, Hong C F, Zhao X R, Fang Y H and Dai P Q 2022 *Ceram. Int.* **48** 30826

[25] Zhao N N, Li Y S, Zhao X X, Zhi X K and Liang G C 2016 *J. Alloys Compd.* **683** 123

[26] Anand K S, Sitaram S R, Raj R, Das A, Goswami D and Das J 2024 *Trans. Indian Inst. Met.* **77** 1529

[27] Suryanarayana C 2001 *Prog. Mater. Sci.* **46** 1